

High-Performance Integrated RF-MEMS: Part 2- Switches

Arthur S. Morris III, Shawn Cunningham[†], Dana Dereus[†], Joseph Repke

wiSpry Inc.
Cary, NC; [†]Colorado Springs, CO

Abstract RF MEMS have been pursued for more than a decade as a solution to the challenge of providing high-performance on-chip switches. This paper presents design and measurement of switches that have unprecedented performance for switches on low-resistivity silicon substrates. The switches have an insertion loss of < 0.2 dB at 4 GHz and < 0.9 dB at 26.5 GHz combined with isolation of > 55 dB at 4 GHz and > 40 dB at 26.5 GHz. This work has been implemented in a process that supports a wide range of applications, allows integration with active circuits, provides high reliability, enables wafer-level packaging and actuation at low supply voltages.

I. INTRODUCTION

RF-MEMS hold great promise for improving performance and increasing the integration of the RF front-end of wireless systems. Many high-performance devices have been built using RF-MEMS. This includes a range of shunt and series switches [1,2,3]. However, none of these has reached commercial success. There are several key challenges to the commercialization of RF-MEMS switches. These include low-cost hermetic or near-hermetic packaging to protect the MEMS and to provide a controlled environment for the contact surfaces. Another key challenge for switches that provide DC contact is the need for metals with the right combination of low contact resistance and low contact adhesion. The third challenge is clearly demonstrating the required reliability for the applications in the range of environments where they will be used. The fourth challenge is operation at low voltages (< 3 V for handset and other portable applications). The fifth challenge is accomplishing all of the above and still providing a cost-effective solution. This paper presents switches that address all of these challenges. Their design and process enables wafer-level packaging and direct integration with active electronics for control of the MEMS as well as functional integration with RF circuitry. While space does not permit details on all of these aspects in this paper, we outline some of our design and modeling approaches along with comparisons to measured data.

II. ELECTROMECHANICAL DESIGN AND MODELING

Several areas are critical to the design of MEMS RF switches. The core of the switch is the RF contacts. These must provide low resistance at a force that can be achieved using the chosen actuation mechanism while easily opening when this force is removed. The open contact gap must be sufficient to provide the required RF isolation. Next in importance is the actuator, which varies the switch contact gap and generates the switch contact force. This must consume negligible power and enable fast switching. It should also be electrically isolated from the RF path through the switch to simplify biasing, reduce radiation, and improve RF performance. The last important area is the RF interconnects to and from the RF contacts. The interconnect must provide very low loss to enable the high performance of the low-resistance contacts to be utilized in an external circuit. The interconnect transitions near the switch contacts also have a strong influence on the resulting isolation.

In a companion paper we have outlined our RF-MEMS process and its benefits. The process and the material properties determined from test structure extractions have been captured in CoventorWare[™] for visualization and modeling of the 3D structure leading to straightforward electromechanical, damping and thermal simulations using CoventorWare[™] and RF analyses using Ansoft's HFSS[™].

Various switch designs were optimized for RF performance and actuation at 20V considering:

- Contact force for repeatable low contact resistance
- Release force to overcome contact adhesion
- Variations in manufacturing stress and stress gradients
- Variations in temperature
- RF insertion loss
- RF isolation
- Substrate effects
- Robustness to over-voltage

The designs illustrated here are basic cantilever beam switches but the principles and design principles have been used for a wide variety of switch designs.

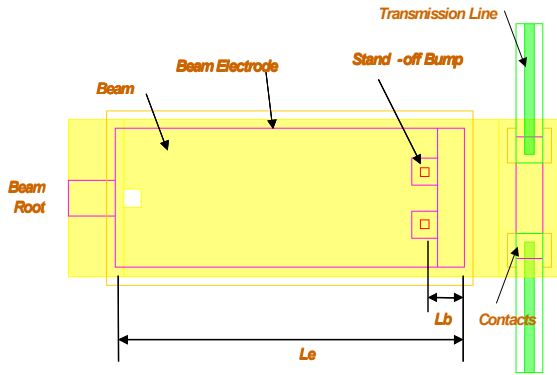


Figure 1 – Basic cantilever switch layout.

Figure 1 shows the cantilever switch layout. Detailed electromechanical simulations were conducted to develop design curves including those that demonstrate the dependency of performance on the switch length, width, thickness and gap. The pull-in voltage as a function of actuation electrode length is shown in Figure 2 for several switch widths. Note that the pull-in voltage is largely independent of the switch width. The pull-in voltage is shown to follow the expected trend as a function of the product of the switch thickness and air gap raised to the power of 1.5 in Figure 3.

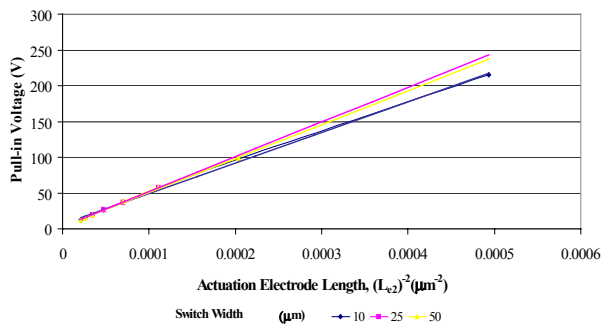


Figure 2 – Pull-in voltage versus the actuation electrode length of the switch.

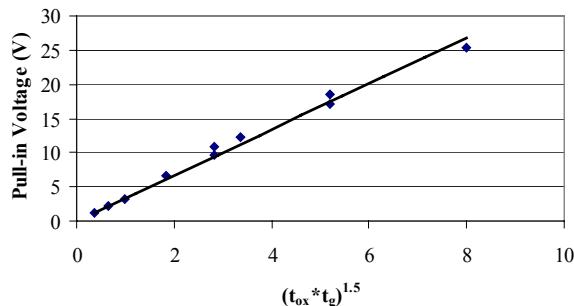


Figure 3 – Pull-in voltage versus the switch thickness times the air gap raised to the power of 1.5.

Next we examine the contact force and the contact separation/breaking force. The contact force must be sufficient to achieve a stable contact resistance, the value

of which depends on the metallurgy. The contact force is shown as a function of the beam width and actuation voltage in Figure 4. Note that a wider cantilever beam is very attractive to increasing contact force.

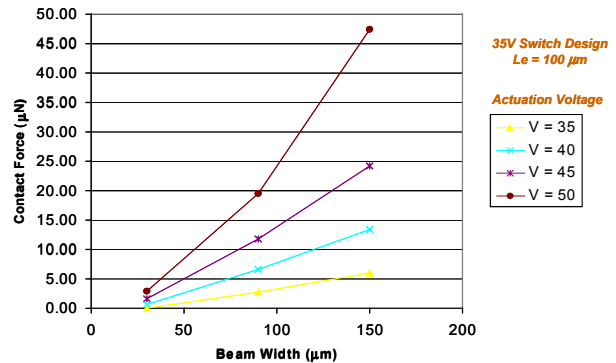


Figure 4 – Contact force versus actuation voltage and beam width at a beam length of 100 µm.

Contact separation/breaking force is critical in Au-based contacts as their adhesion can be quite high [4]. This was simulated in two ways: tip contact and flush contact. In tip contact, only the leading edge of the moving contact is in contact, so the stored elastic energy is lower than for the flush contact. However, the flush contact provides the lowest resistance and the most adhesion. The model for the flush contact analysis is shown in Figure 5. The flush contact breaking force is shown as a function of switch length in Figure 6.

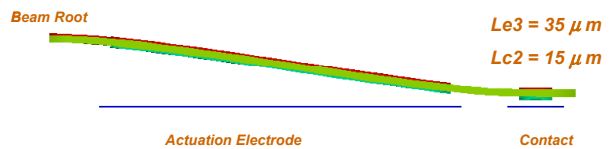


Figure 5 – Switch side view showing flush contact for estimating flush contact breaking force.

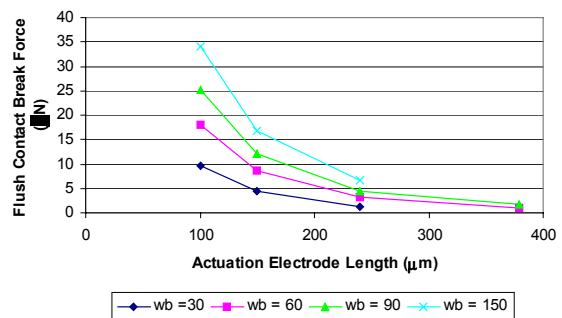


Figure 6 – Flush contact breaking force dependency on switch actuation electrode length and beam width.

To enhance the reliability of the switch, isolation standoff bumps are used to prevent control plate shorting. A critical design parameter for the isolation bumps is their

location relative to the edge of the electrode. The goal of the isolation bump design has been to maximize the contact force while still preventing shorting or gas breakdown. In Figure 7, the contact force is shown as a function of the isolation stand-off bump location and actuation voltage for a 100 μm long switch. This shows the contact force can be enhanced by locating the isolation bumps 20 μm behind the edge of the electrode.

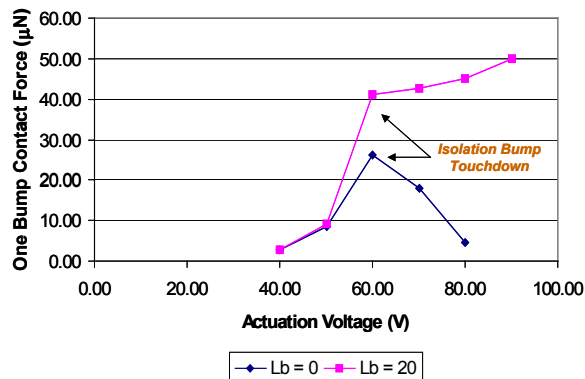


Figure 7 – Contact force on a single contact bump versus actuation voltage and isolation stand-off bump location for a 100 μm long electrode.

III. RF MODELING AND MEASUREMENTS

Figure 8 shows the solid model of the RF switch, which is directly imported into an Ansoft HFSS 3-D model from the native .SAT file. Then the RF designs were analyzed in HFSS as well as with equivalent circuits in Agilent's ADS.

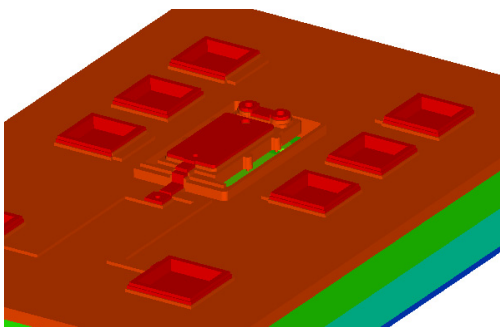


Figure 8 – Solid model of RF-switch with vertical axis expanded 10x.

HFSS simulation showed lower insertion loss than measured results as contact resistance was not included. Using ADS, a contact resistance of 0.5 ohm per contact was added to each model to empirically compensate the simulations to match the measured results. The results for all five cases (measured vs the simulations with and without contact resistance) are shown below in Figure 9.

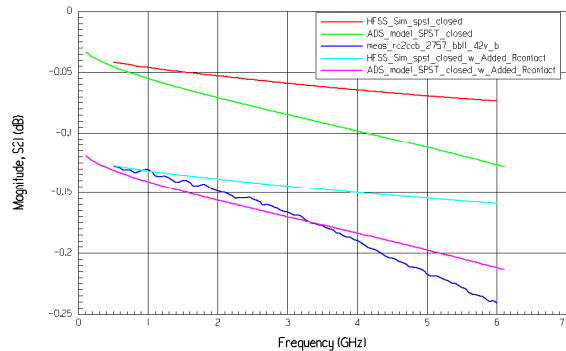


Figure 9 – Switch Insertion Loss: Measured Data vs HFSS Simulations vs ADS Equivalent-Circuit Model

Plots of switch isolation are displayed in Figure 10 with simulations showing good agreement with the measured data although the measured isolation was higher due to a larger than nominal contact gap. Measured isolation was approximately 62 dB at 2 GHz, and 52 dB at 6 GHz.

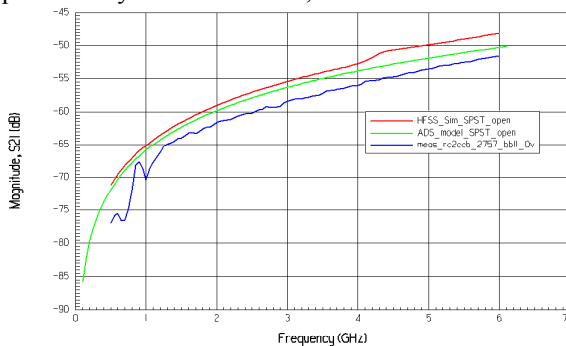


Figure 10 – Isolation of Switch : Measured data vs HFSS Simulation vs ADS Equivalent-Circuit Model

Measurements to extended frequencies show good RF performance continuing to 26.5 GHz with insertion loss < 0.9 dB and isolation > 40 dB.

IV. CONCLUSION

We have presented some details of the design and experimental results of a high-performance RF-MEMS switch built in a standardized flexible process on low-resistivity silicon with insertion loss < 0.2 dB and isolation > 55 dB at 4 GHz.

REFERENCES

- [1] G.-L. Tan and G. M. Rebeiz, "A DC-Contact MEMS shunt switch," IEEE microwave and wireless components letters, Vol. 12, No. 6, June 2002, pp. 212-214.
- [2] J. J. Yao and M. F. Chang, "A surface micromachined miniature switch for telecommunications applications with signal frequencies from dc up to 4GHz," Transducers 95 Eurosensors IX, Th 8th Intl. Conf. on Solid-State Sensors and Actuators, Stockholm, Sweden, June 25-29, 1995, pp. 384-387.
- [3] C. Goldsmith, et al., "Characteristics of micromachined switches at microwave frequencies," 1996 IEEE MTT-S Digest, pp. 1141-1144.
- [4] Schimkat, J., "Contact measurements providing basic design data for microrelay actuators," Sensors and Actuators, 73 (1999) 138-143.